nature physics

LETTERS

https://doi.org/10.1038/s41567-019-0535-3

Avoided quasiparticle decay from strong quantum interactions

Ruben Verresen[1,2,3]*, Roderich Moessner[1] and Frank Pollmann[2,4]

Quantum states of matter—such as solids, magnets and topological phases—typically exhibit collective excitations (for example, phonons, magnons and anyons)[1]. These involve the motion of many particles in the system, yet, remarkably, act like a single emergent entity—a quasiparticle. Known to be long lived at the lowest energies, quasiparticles are expected to become unstable when encountering the inevitable continuum of many-particle excited states at high energies, where decay is kinematically allowed. Although this is correct for weak interactions, we show that strong interactions generically stabilize quasiparticles by pushing them out of the continuum. This general mechanism is straightforwardly illustrated in an exactly solvable model. Using state-of-the-art numerics, we find it at work in the spin-1⁄2 triangular-lattice Heisenberg antiferromagnet (TLHAF). This is surprising given the expectation of magnon decay in this paradigmatic frustrated magnet. Turning to existing experimental data, we identify the detailed phenomenology of avoided decay in the TLHAF material[2] $Ba_3CoSb_2O_9$, and even in liquid helium[3–8], one of the earliest instances of quasiparticle decay[9]. Our work unifies various phenomena above the universal low-energy regime in a comprehensive description. This broadens our window of understanding of many-body excitations, and provides a new perspective for controlling and stabilizing quantum matter in the strongly interacting regime.

It is a fundamental insight of quantum mechanics that energy levels repel. This is commonly illustrated by letting two levels with unperturbed ('bare') energies $\pm E_b$ interact with one another through a coupling γ:

$$\hat{H} = \begin{pmatrix} E_b & \gamma \\ \gamma & -E_b \end{pmatrix} \tag{1}$$

The resulting energies of $\hat{H}$ are $\pm\sqrt{E_b^2+\gamma^2}$. Hence, repulsion leads to a minimal separation of the levels of $2|\gamma|$, no matter how small the initial separation $2|E_b|$.

A natural question is whether this extends to the case of a discrete level coupled to a continuum of states. The question might seem moot, because the common expectation is that a bare level inside a continuum will be dissolved by interactions. At best, it will become a finite-lifetime resonance. At worst, no hint of it remains.

If the bare level represents a quasiparticle, its broadening and disappearance in the many-particle continuum is known as quasiparticle decay. In the case of non-topological quantum magnets (for a detailed review, see ref. [10])—where quasiparticles go under the name of magnons or spin waves—the expectation of magnon decay has, surprisingly only recently, been borne out in inelastic neutron scattering experiments[11–15] (see below).

We show that this expectation of quasiparticle decay is wrong if interactions are strong. Rather, with increasing interaction strength, an infinitely long-lived state re-emerges out of the continuum of states. This happens via a simple generalization of the familiar level repulsion, equation (1), for a bare state $|\psi\rangle$ with bare energy E_b coupled to a continuum of states $|\varphi_\alpha\rangle$ with bare energies E_α above a threshold energy E_{th}. Physically, this model represents states with a fixed value of total momentum (the continuous index α corresponds to the relative momentum of two-particle states).

Concretely, for large enough coupling $|\gamma|$, there is a single discrete state $|\psi^\star\rangle$ with an energy below the continuum, $E^\star < E_{th}$ (see Methods). Moreover, the contribution of the unperturbed state $|\psi\rangle$ to this final discrete state, denoted by the weight $Z = |\langle\psi|\psi^\star\rangle|^2$, can be large, and the weight approaches $Z \to \frac{1}{2}$ for large $|\gamma|$ if the continuum has finite support.

This is experimentally important: a vanishing Z implies that the state $|\psi^\star\rangle$ bears little relationship to the original quasiparticle. However, a large Z ensures that any experimental set-up for detecting the original quasiparticle $|\psi\rangle$ also detects $|\psi^\star\rangle$. Hence, while the existence of $|\psi^\star\rangle$ and finiteness of Z for this simple model have been pointed out before[16], its phenomenology, and in particular its relevance to quasiparticles in strongly interacting quantum systems, seems to have been under-appreciated.

Figure 1 illustrates what inelastic neutron scattering would measure for a system described by this solvable model (see Methods). It shows the weight of the bare state $|\psi\rangle$ on the true eigenstates. The initially flat bare level (dashed line) is coupled to a continuum (shaded region). For weak interactions, the physics depends on the number of states the bare level encounters on entering the continuum. This is encoded in the density of states (DOS), $\nu(E)$. In this example we treat the case of the two-particle continuum of non-interacting particles with a parabolic dispersion (although any dispersion can be accommodated); its onset satisfies $\nu(E_{th}+\delta E) \approx (\delta E)^{D/2-1}$ in D spatial dimensions (see Supplementary Information).

We first discuss weak coupling γ. In high dimensions ($D \geq 3$), the quasiparticle straightforwardly enters the continuum and decays (Fig. 1, top right). In lower dimensions, the entrance behaviour is delicate. For our particular model, the state cannot enter the continuum at all due to the discontinuous onset of the DOS[16]. Instead, its spectral weight Z is transferred into a decaying mode in the continuum. Detecting the residual quasiparticle requires very sensitive and high-resolution measurements (for example, neutron spin echo spectroscopy; see below). This singular behaviour may be regularized in a more complete model, allowing the state to terminate[9], which need not affect Fig. 1 (top left) at the resolution shown.

[1]Max-Planck-Institute for the Physics of Complex Systems, Dresden, Germany. [2]Department of Physics, Technische Universität München, Garching, Germany. [3]Kavli Institute for Theoretical Physics, University of California, Santa Barbara, CA, USA. [4]Munich Center for Quantum Science and Technology (MCQST), Munich, Germany. *e-mail: rubenverresen@gmail.com

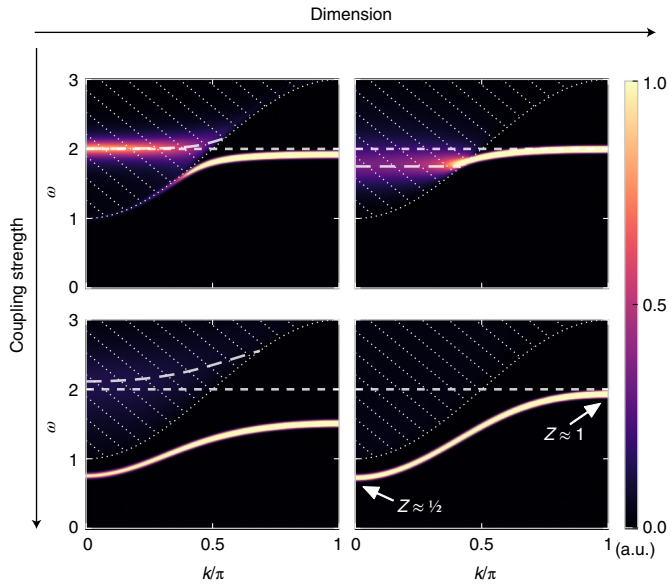

Fig. 1 | Avoided quasiparticle decay in a solvable model. The bare level $|\psi_k\rangle$ (horizontal short-dashed line) is coupled to a continuum (hashed dotted lines). The left (right) column is representative of a continuum of gapped particles in dimensions $D=1$, 2 ($D\geq 3$). At weak coupling, we observe a decaying mode in the continuum (long-dashed line), with near-entrance behaviour depending on the dimensionality. For strong interactions, the outcome is independent of dimension: a renormalized quasiparticle $|\psi_k^\star\rangle$ is pushed out, whose weight $Z_k=|\langle\psi_k|\psi_k^\star\rangle|^2$ approaches $\frac{1}{2}$.

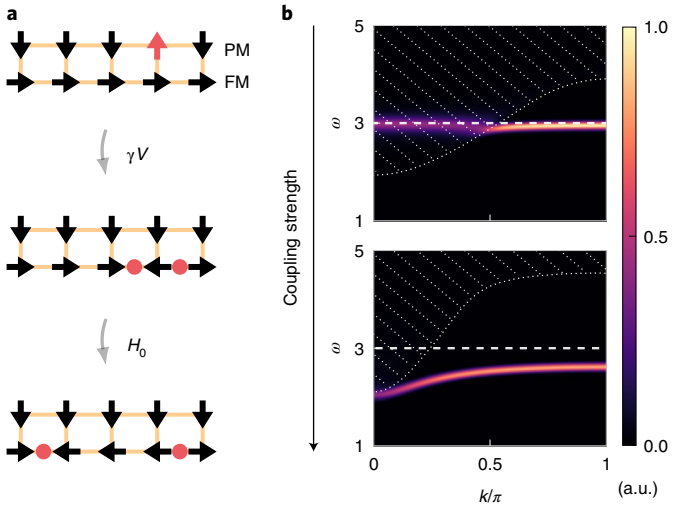

Fig. 2 | Avoided decay in an Ising ladder. a, A paramagnet (PM) with magnon-like excitation (red arrow) and an Ising ferromagnet (FM) where the quasiparticles are domain walls. By coupling the two chains, a magnon can decay into two domain walls (red dots). **b**, The dynamic structure factor. The horizontal dashed line is the bare magnon dispersion (set by $\hat{H}_0^{(A)}$) and the shaded region (dotted lines) denotes the continuum of two domain walls (kinematic combinations of the numerically obtained dispersion). At low coupling strength, the magnon decays. For strong interactions, the magnon is pushed below the continuum.

The main focus of the present work is on large coupling γ, where we find that the quasiparticle re-emerges for any D (Fig. 1, bottom), accompanied by the weight $Z\to\frac{1}{2}$, in agreement with our general claim.

How widely applicable is this mechanism of avoided quasiparticle decay? Note that the fact we assumed γ to be independent of α is not important, because in the full solution, γ^2 and the DOS always appear together. For example, in a system with $SO(3)$ spin symmetry, the coupling constant vanishes near the threshold as $\gamma(E_{\rm th}+\delta E)\approx\sqrt{\delta E}$ (ref. [17]). This leads to a different power of the onset of $\gamma^2\nu(E)$, which amounts to shifting the effective dimensionality $D\to D+2$. Similarly, one could effectively include direct interactions within the continuum by using a renormalized DOS.

There are, however, two essential implicit assumptions. First, there is space below the continuum into which to be repelled. This is not applicable to Fermi liquids, for example, where the continuum starts directly above the ground-state energy over an extended region in momentum space. Second, the model does not actually treat the situation where the continuum is made of the same quasiparticles that it repels, making it exactly solvable. This should be a good approximation if the quasiparticle trying to enter the continuum has its momentum $\mathbf{k}$ well-separated from those quasiparticles whose momenta $\mathbf{q}$ and $\mathbf{k}-\mathbf{q}$ make up the continuum at that point. As discussed below, this turns out to be the case in the TLHAF.

Before considering the challenging TLHAF, we verify our predictions in a tunable, yet numerically tractable, fully many-body quantum system. This consists of two spin-$\frac{1}{2}$ chains: one a perfect paramagnet in a field, $\hat{H}_0^{(A)}=-3\sum_n\hat{S}^z_{A,n}$, the other an ordered quantum Ising ferromagnet, $\hat{H}_0^{(B)}=-\sum_n(4J\hat{S}^x_{B,n}\hat{S}^x_{B,n+1}+2g\hat{S}^z_{B,n})$. The ground state of the paramagnet has all spins pointing up (a flipped spin is a dispersionless magnon). The ferromagnet is ordered along the x direction, with freely moving domain wall quasiparticles.

Inter-chain coupling can allow the magnon to decay into a pair of domain walls, illustrated in Fig. 2a. For this, consider the interaction $H_{\rm int}=4\gamma\sum_n\hat{S}^x_{A,n}\hat{S}^z_{B,n}$. Our numerical data obtained using the dynamical density matrix renormalization group method (DMRG)[18–20] (Fig. 2b) confirms the resulting familiar magnon decay for weak interactions. Crucially, as advertised, strong interactions prevent quasiparticle decay, and the magnon re-emerges from the continuum unscathed. For precise values of the parameters, see Methods.

We now turn to the paradigmatic spin-$\frac{1}{2}$ TLHAF, which describes a wide range of frustrated quantum spin materials (see ref. [21] for a recent overview). Its ground state is ordered, with neighbouring spins forming a 120° angle[22,23]. However, away from the lowest energies[24], the status of its magnon excitations remains unsettled due to the uncontrolled nature of the available analytic and numerical methods[10,24–26]. The most venerable of these is perhaps spin wave theory (SWT), an expansion in inverse spin, $1/S$.

We consider the spin-$\frac{1}{2}$ TLHAF

$$\hat{H}=J\sum_{\langle\mathbf{n},\mathbf{m}\rangle}\left((1-\delta)\,\hat{\mathbf{S}}_\mathbf{n}\cdot\hat{\mathbf{S}}_\mathbf{m}-\frac{\delta}{2}\hat{S}^{\rm loc,z}_\mathbf{n}\hat{S}^{\rm loc,z}_\mathbf{m}\right)\qquad(2)$$

where a small easy-axis anisotropy ($\delta=0.05$) slightly gaps out the massless Goldstone modes, making the model more numerically tractable. Here, $\hat{\mathbf{S}}^{\rm loc}_\mathbf{n}$ is the spin in the basis of the rotating (local) frame.

For this value of δ, SWT predicts magnon decay[24] over a large region of momentum space (region shaded with dotted lines in the inset of Fig. 3a). A magnon with momentum $\mathbf{k}$ is then predicted to decay into two magnons with momenta $\mathbf{q}$ and $\mathbf{k}-\mathbf{q}$, where $\mathbf{q}\approx$ K, the corner of the Brillouin zone. However, small spin and non-collinear order—breaking all symmetries and thus allowing for many interaction terms—generate strong quantum interactions. This suggests an alternative to the expected scenario of magnon decay.

A recent advance in numerically simulating the dynamics of two-dimensional (2D) quantum systems[27,28] allows us to directly test the prediction of magnon decay in equation (2). Figure 3a shows the out-of-plane dynamical spin structure factor along the A–B line

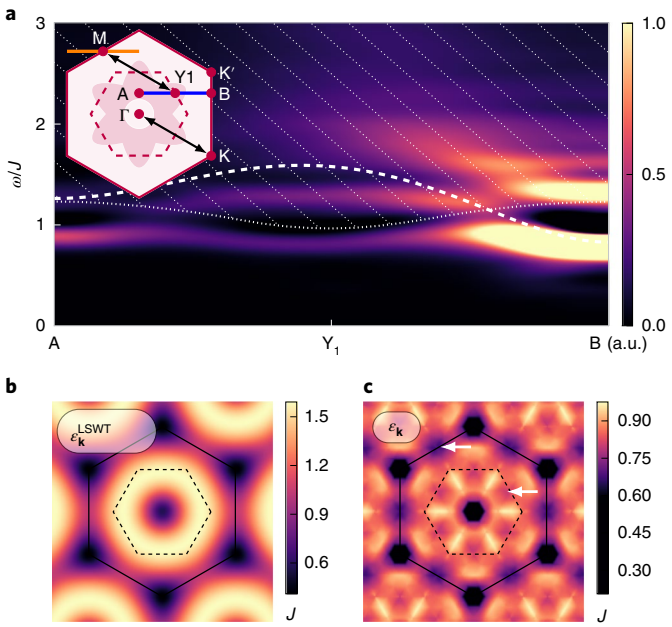

Fig. 3 | Avoided decay in the spin-$\frac{1}{2}$ TLHAF with $\delta = 0.05$. a, Inset: the Brillouin zone (the dashed line delineates the magnetic Brillouin zone). Linear spin wave theory (LSWT) predicts magnon decay in the shaded region, dominated by the process $\mathbf{q} \rightarrow (\mathbf{q} - \mathrm{K}) + \mathrm{K}$. The black arrows illustrate that $\mathrm{Y}_1 = \mathrm{M} + \mathrm{K}$; hence decay is possible if $\varepsilon_{\mathrm{Y}_1} > \varepsilon_{\mathrm{M}} + \varepsilon_{\mathrm{K}}$. Main panel: the out-of-plane dynamical spin structure factor along the blue line in the inset. The dotted line represents the two-magnon states consisting of a magnon along the orange line (inset) and a K-magnon. The dashed line is the magnon dispersion from LSWT. We see avoided decay, where the level-continuum repulsion induces a local minimum near Y_1. **b**,**c**, The LSWT prediction for the dispersion relation (**b**) and the numerical result (**c**). The dispersion is most heavily renormalized where LSWT predicts decay (see inset of **a**). The local minimum at M induces a local minimum at Y_1 (white arrows).

(blue line, inset) obtained from dynamical DMRG (see Methods). Becaue SWT predicts decay into a K-magnon, the dotted line shows the numerically obtained two-magnon energy $\varepsilon_{\mathbf{q}} + \varepsilon_{\mathrm{K}}$, with $\mathbf{q}$ along the orange line in the inset. The dashed curve is the SWT prediction of the magnon in the non-interacting limit $1/S \rightarrow 0$ (LSWT), travelling deep into the two-magnon continuum. However, the numerically obtained $S = \frac{1}{2}$ dispersion is pushed out completely—a crisp instance of avoided magnon decay.

The dispersion is known to have a local minimum at the midpoint M of the Brillouin zone edge. This appears at higher order in SWT and in series expansion methods[24–26], as confirmed in Fig. 3c. Our novel prediction is that the avoided decay must in turn induce a local minimum at the midpoint Y_1 of the magnetic Brillouin zone edge. This is apparent in Fig. 3a,c. More precisely, absence of magnon decay implies the strong constraint $|\varepsilon_{\mathrm{M}} - \varepsilon_{\mathrm{Y}_1}| \leq \varepsilon_{\mathrm{K}}$, which we find to be satisfied in our numerics, and in disagreement with SWT.

Intriguingly, this phenomenology has already been observed in experiments. The magnetic material $Ba_3CoSb_2O_9$ is well described by the TLHAF with a small easy-plane anisotropy. Figure 4a shows recent inelastic neutron scattering data[2]. Because this is sensitive to the full dynamical spin structure factor, it picks up copies of the magnon dispersion translated by K. Figure 4a thus shows two bands: the bottom one (ε_1) centred at M and the top one (ε_2) centred at Y_1. Neither decay, and both exhibit a local minimum, in agreement with the phenomenology of Fig. 3. For comparison, Fig. 4b shows the numerically obtained data for the model described by equation (2) along the same momentum cut (see Supplementary Information). We can thus directly reinterpret apparently unrelated experimental features as being linked through avoided quasiparticle decay.

In contrast, magnon decay has been observed experimentally in a spin-2 TLHAF[13]. This is consistent with $1/S$ being a measure of the interaction strength, and avoided decay requiring strong interactions.

Level–continuum repulsion was also recently observed[29] in the gapped spin–orbit-coupled frustrated magnet $BiCu_2PO_6$. This nicely fits our theoretical framework: its 1D nature suggests a sharp discontinuous onset of the bare two-magnon DOS $(\gamma^2 \nu(E_{\mathrm{th}} + \delta E) \approx 1/\sqrt{\delta E})$, preventing a smooth quasiparticle entry into the continuum.

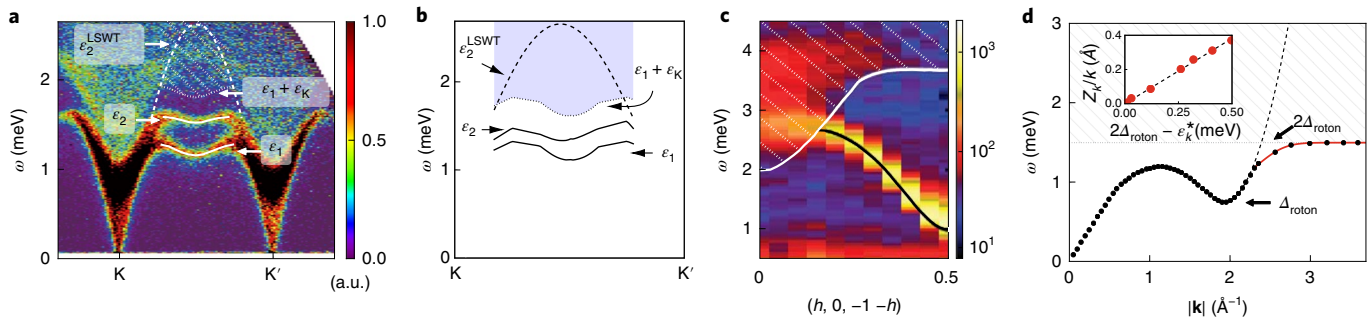

Fig. 4 | Avoided quasiparticle decay, genuine decay and level–continuum repulsion in experimental data for the TLHAF material $Ba_3CoSb_2O_9$, piperazinium hexachlorodicuprate (PHCC) and superfluid helium. a, Inelastic neutron scattering data and LSWT comparison for $Ba_3CoSb_2O_9$ (see Methods for details)[2]. The neutron data pick up all magnon bands related by momentum K; the lower branch (ε_1) goes through M, the higher branch (ε_2) through Y_1 (see Fig. 3 for Brillouin zone labelling). Similar to Fig. 3, magnon decay is avoided, with the local minimum near M inducing a local minimum near Y_1. **b**, For comparison, we show the numerically obtained dispersion for the model described by equation (2) with $\delta = 0.05$, taking $J = 1.67$ meV as in ref. [2] and including bands related by momentum K. We stress that this Hamiltonian does not directly model the experiment: the former (latter) has a small easy-axis (easy-plane) anisotropy. The similarity between **a** and **b** is evidence of the robustness of our proposed mechanism. **c**, A scenario where the quasiparticle does decay: inelastic neutron scattering data[11] for PHCC. The white shaded region denotes the two-magnon continuum. The black line traces the magnon, which decays into the continuum. **d**, Black dots are the phonon–roton dispersion of superfluid helium extracted from refs. [4,5]. Inset: single-particle weight extracted from refs. [6,7] (see Methods). Our solvable model implies that the level approaches the continuum exponentially in the bare level: $E_k^\star \propto -\exp(-b \times k \times E_k^{\mathrm{bare}})$ (solid red line). Here, $E_k^\star := \varepsilon_k^\star - 2\Delta_{\mathrm{roton}}$ and $E_k^{\mathrm{bare}} := \varepsilon_k^{\mathrm{bare}} - 2\Delta_{\mathrm{roton}}$, with the bare level $\varepsilon_k^{\mathrm{bare}}$ estimated by fitting the roton minimum to a parabola. Moreover, the weight is predicted to go to zero proportional to the level approaching the continuum, that is, $Z_k \approx a \times k \times |E_k^\star|$, as confirmed in the inset. In both cases, we find that $a_{\mathrm{fit}}\ k_{\mathrm{roton}}$ and $b_{\mathrm{fit}}\ k_{\mathrm{roton}}$ are comparable to the (inverse) bandwidth, in testament to the strong interactions.

This is in contrast to the quasiparticle decay observed[11] in the 2D PHCC. Because the latter is spin–rotation symmetric, our earlier argument implies the effective dimensional shift $D=2\rightarrow D=4$. Hence, $\gamma^2\nu(E_{\mathrm{th}}+\delta E)\approx\delta E$, consistent with the smooth entry in Fig. 4c.

Finally, we consider the iconic quasiparticle dispersion of superfluid helium (Fig. 4d). Although it was originally thought that the quasiparticle would enter the two-roton continuum[9], it is now known that the dispersion instead flattens off, consistent with the discontinuous onset of the two-roton DOS[3,8] (see Supplementary Information). Here, we add the following quantitative insights. First, the distance to the continuum is exponentially small in the bare energy (red curve). Second, the quasiparticle weight Z decays to zero linearly with this distance; the high-quality data of refs. [4–7] allow us to extract this information to confirm this prediction (inset, Fig. 4c). In fact, these two seemingly unrelated predictions are unified in our theory via the Hellmann–Feynman theorem, yielding $\mathrm{d}E^*/\mathrm{d}E_{\mathrm{b}}=Z$ (see Methods). Incidentally, avoided decay can also be found for smaller momenta[30].

In conclusion, away from the universal low-energy regime, the excitations of many-body systems are not as unstructured as perhaps expected. Aside from the general message that interactions can prevent or even undo quasiparticle decay, our model can be used to derive functional relationships between a priori unrelated quantities to extract fundamentally interesting information such as the strength of interactions from experiment, as showcased for superfluid helium. Our work also implies that the existence of quasiparticle decay is not the default option, but instead places considerable constraints on underlying physical processes.

All of these insights, taken together, suggest the possibility of using interactions to control, in particular to stabilize, the behaviour of quantum matter by employing, rather than combatting, strong interactions.

Online content

Any methods, additional references, Nature Research reporting summaries, source data, statements of code and data availability and associated accession codes are available at https://doi.org/10.1038/s41567-019-0535-3.

Received: 9 October 2018; Accepted: 13 April 2019;
Published online: 27 May 2019

References

1. Liesbeth, V. et al. The quasiparticle zoo. *Nat. Phys.* **12**, 1085–1089 (2016).
2. Ito, S. et al. Structure of the magnetic excitations in the spin-1/2 triangular-lattice Heisenberg antiferromagnet $Ba_3CoSb_2O_9$. *Nat. Commun.* **8**, 235 (2017).
3. Woods, A. D. B. & Cowley, R. A. Structure and excitations of liquid helium. *Rep. Prog. Phys.* **36**, 235 (1973).
4. Donnelly, J. A. & Hills, R. N. Specific heat and dispersion curve for helium II. *J. Low Temp. Phys.* **44**, 471–489 (1981).
5. Glyde, H. R., Gibbs, M. R., Stirling, W. G. & Adams, M. A. Excitations in superfluid ^{4}He beyond the roton. *Europhys. Lett.* **43**, 422–426 (1998).
6. Gibbs, M. R., Andersen, K. H., Stirling, W. G. & Schober, H. The collective excitations of normal and superfluid ^{4}He: the dependence on pressure and temperature. *J. Phys. Condens. Matter.* **11**, 603–628 (1999).
7. Azuah, R. T., Diallo, S. O., Adams, M. A., Kirichek, O. & Glyde, H. R. Phonon–roton modes of liquid ^{4}He beyond the roton in the porous medium MCM-41. *Phys. Rev. B* **88**, 024510 (2013).
8. Glyde, H. R. Excitations in the quantum liquid ^{4}He: a review. *Rep. Prog. Phys.* **81**, 014501 (2018).
9. Pitaevskii, L. P. Properties of the spectrum of elementary excitations near the disintegration threshold of the excitations. *J. Exp. Theor. Phys.* **9**, 830 (1959).
10. Zhitomirsky, M. E. & Chernyshev, A. L. Colloquium: spontaneous magnon decays. *Rev. Mod. Phys.* **85**, 219–242 (2013).
11. Stone, M. B., Zaliznyak, I. A., Hong, T., Broholm, C. L. & Reich, D. H. Quasiparticle breakdown in a quantum spin liquid. *Nature* **440**, 187–190 (2006).
12. Masuda, T. et al. Dynamics of composite haldane spin chains in IPA–$CuCl_3$. *Phys. Rev. Lett.* **96**, 047210 (2006).
13. Oh, J. et al. Magnon breakdown in a two-dimensional triangular lattice Heisenberg antiferromagnet of multiferroic $LuMnO_3$. *Phys. Rev. Lett.* **111**, 257202 (2013).
14. Robinson, N. J., Essler, F. H. L., Cabrera, I. & Coldea, R. Quasiparticle breakdown in the quasi-one-dimensional Ising ferromagnet $CoNb_2O_6$. *Phys. Rev. B* **90**, 174406 (2014).
15. Hong, T. et al. Field induced spontaneous quasiparticle decay and renormalization of quasiparticle dispersion in a quantum antiferromagnet. *Nat. Commun.* **8**, 15148 (2017).
16. Gaveau, B. & Schulman, L. S. Limited quantum decay. *J. Phys. A.* **28**, 7359–7374 (1995).
17. Zhitomirsky, M. E. Decay of quasiparticles in quantum spin liquids. *Phys. Rev. B* **73**, 100404 (2006).
18. White, S. R. Density matrix formulation for quantum renormalization groups. *Phys. Rev. Lett.* **69**, 2863–2866 (1992).
19. Schollwöck, U. The density-matrix renormalization group in the age of matrix product states. *Ann. Phys.* **326**, 96–192 (2011).
20. Zaletel, M. P., Mong, R. S. K., Karrasch, C., Moore, J. E. & Pollmann, F. Time-evolving a matrix product state with long-ranged interactions. *Phys. Rev. B* **91**, 165112 (2015).
21. Kojima, Y. et al. Quantum magnetic properties of the spin-$\frac{1}{2}$ triangular-lattice antiferromagnet $Ba_2La_2CoTe_2O_{12}$. *Phys. Rev. B* **98**, 174406 (2018).
22. Huse, D. A. & Elser, V. Simple variational wave functions for two-dimensional Heisenberg spin-$\frac{1}{2}$ antiferromagnets. *Phys. Rev. Lett.* **60**, 2531–2534 (1988).
23. Bernu, B., Lhuillier, C. & Pierre, L. Signature of Néel order in exact spectra of quantum antiferromagnets on finite lattices. *Phys. Rev. Lett.* **69**, 2590–2593 (1992).
24. Chernyshev, A. L. & Zhitomirsky, M. E. Spin waves in a triangular lattice antiferromagnet: decays, spectrum renormalization and singularities. *Phys. Rev. B* **79**, 144416 (2009).
25. Zheng, W., Fjærestad, J. O., Singh, R. R. P., McKenzie, R. H. & Coldea, R. Excitation spectra of the spin- $\frac{1}{2}$ triangular-lattice Heisenberg antiferromagnet. *Phys. Rev. B* **74**, 224420 (2006).
26. Mourigal, M., Fuhrman, W. T., Chernyshev, A. L. & Zhitomirsky, M. E. Dynamical structure factor of the triangular-lattice antiferromagnet. *Phys. Rev. B* **88**, 094407 (2013).
27. Gohlke, M., Verresen, R., Moessner, R. & Pollmann, F. Dynamics of the Kitaev–Heisenberg model. *Phys. Rev. Lett.* **119**, 157203 (2017).
28. Verresen, R., Pollmann, F. & Moessner, R. Quantum dynamics of the square-lattice Heisenberg model. *Phys. Rev. B* **98**, 155102 (2018).
29. Plumb, K. W. et al. Quasiparticle-continuum level repulsion in a quantum magnet. *Nat. Phys.* **12**, 224–229 (2016).
30. Bhatt, R. N. & McMillan, W. L. Theory of anomalous dispersion in liquid He^4. *Phys. Rev. A* **10**, 1591–1597 (1974).
31. Demkov, Y. N. & Osherov, V. I. Stationary and nonstationary problems in quantum mechanics that can be solved by means of contour integration. *Sov. J. Exp. Theor. Phys.* **26**, 916 (1968).
32. Basko, D. M. Landau–Zener–Stueckelberg physics with a singular continuum of states. *Phys. Rev. Lett.* **118**, 016805 (2017).

Acknowledgements

The authors thank R. Coldea, S. Parameswaran and S. Chernyshev for discussions, and the latter for detailed comments on the manuscript. The authors also thank I. Khaymovich for pointing out the inspiring refs. [31,32]. R.V. was supported by the German Research Foundation (DFG) through the Collaborative Research Center SFB 1143. F.P. acknowledges support from DFG Research Unit FOR 1807 through grant no. PO 1370/2-1, TRR80, Nanosystems Initiative Munich (NIM) by the German Excellence Initiative, the DFG under Germany's Excellence Strategy EXC-2111-390814868, and the European Research Council (ERC) under the European Union's Horizon 2020 research and innovation programme (grant agreement no. 771537). This research was supported in part by the National Science Foundation under grant no. NSF PHY-1748958 and by the Heising–Simons Foundation.

Author contributions

All authors contributed equally to this work.

Competing interests

The authors declare no competing interests.

Additional information

Supplementary information is available for this paper at https://doi.org/10.1038/s41567-019-0535-3.

Reprints and permissions information is available at www.nature.com/reprints.

Correspondence and requests for materials should be addressed to R.V.

Publisher's note: Springer Nature remains neutral with regard to jurisdictional claims in published maps and institutional affiliations.

Methods

Exactly solvable model. We couple a bare state $|\psi\rangle$ with bare energy E_b to a continuum of states $|\varphi_\alpha\rangle$ with bare energies E_α, that is, $\hat{H}=\hat{H}_0+\gamma\hat{V}$, where

$$\hat{H}_0=E_b\,|\psi\rangle\langle\psi|+\int d\alpha\, E_\alpha|\varphi_\alpha\rangle\langle\varphi_\alpha| \tag{3}$$

$$\hat{V}=\int d\alpha\,(|\psi\rangle\langle\varphi_\alpha|+|\varphi_\alpha\rangle\langle\psi|) \tag{4}$$

The continuous label α satisfies $\langle\varphi_\alpha|\varphi_\beta\rangle=\delta(\alpha-\beta)$ and the density of states of the continuum is denoted as $\nu(E)$. For convenience, we define our origin to be at the onset of the continuum (in the notation of the main text, $E_{th}=0$).

It is useful to consider the single-particle Green's function $G(E)=\langle\psi|(E-\hat{H})^{-1}|\psi\rangle$. One can derive that $G(E)^{-1}=E-E_b-\gamma^2 g(E)$ where we have defined $g(E):=\int\frac{\nu(\varepsilon)}{E-\varepsilon}d\varepsilon$. A detailed derivation can be found in the Supplementary Information. Note that $\lim_{E\to-\infty}G(E)^{-1}=-\infty$ and $\lim_{E\to0^-}G(E)^{-1}=-E_b-\gamma^2 g(0^-)$. Because $G'(E)>0$, the existence of a (unique) pole at E^* below the continuum (that is, $E^*<0$) is equivalent to $G(0^-)^{-1}>0$, which on its turn is equivalent to $\gamma^2>E_b/|g(0^-)|$. If $\nu(0^+)\neq0$ (that is, the DOS has a discontinuous onset), then the integral defining $|g(0^-)|$ diverges, so any non-zero γ will give rise to a pole below the continuum. We note that an equivalent treatment can be found in ref. [16].

To obtain the single-particle weight $Z=|\langle\psi|\psi^*\rangle|^2$ (where $|\psi^*\rangle$ is the wavefunction with energy $E^*<0$), consider that the weight of the delta function $\delta(E-E_b-\gamma^2 g(E))$ is given by the inverse derivative of its argument, that is $Z=\frac{1}{1-\gamma^2 g'(E^*)}$. Moroever, for large $|\gamma|$, we have the relationship $E^*=\gamma^2 g(E^*)$. In particular, from this one can derive that $E^*\to-\infty$ as $|\gamma|\to\infty$. We thus have that

$$\lim_{|\gamma|\to\infty}Z=\lim_{E\to-\infty}\left(1-\frac{E\,g'(E)}{g(E)}\right)^{-1} \tag{5}$$

To evaluate this, we need the asymptotic behaviour of $g(E)$. If $\nu(E)$ has finite support, then $g(E)\approx\frac{1}{E}\int\nu(\varepsilon)d\varepsilon$ as $|E|\to\infty$. Plugging this into equation (5), we obtain $Z\to\frac{1}{2}$ as claimed in the main text.

If $\nu(E)$ is not bounded but instead decays as $\nu(E)\approx\beta/E^\alpha$ with $\alpha>0$ as $E\to+\infty$, then by the theory of Stieltjes this transforms[33]

$$g(E)\approx_{E\to-\infty}\begin{cases}-\widetilde{\beta}/|E|^{\min(1,\alpha)} & \text{if } 0<\alpha\neq1\\ \widetilde{\beta}(\ln|E|)/E & \text{if } \alpha=1\end{cases}\qquad(\widetilde{\beta}>0) \tag{6}$$

From these asymptotics, we obtain

$$\lim_{|\gamma|\to\infty}Z=\begin{cases}1/2 & \text{if } \alpha\geq1,\\ 1/(1+\alpha) & \text{if } 0<\alpha<1.\end{cases} \tag{7}$$

Note that this is lower bounded by $\frac{1}{2}$. In particular, for $\nu(E)\propto1/\sqrt{E}$, we obtain $Z\to\frac{2}{3}$ as $|\gamma|\to\infty$.

In Fig. 1, we plot the weight of the bare state $|\psi\rangle$ on the excited states; that is $\mathcal{A}(E):=\sum_n|\langle\psi|n\rangle|^2\,\delta(E-E_n)$. We calculate it from the identity $\mathcal{A}(E)=\frac{1}{\pi}\mathrm{Im}G(E-i0^+)$. A straightforward calculation (included in the Supplementary Information) gives

$$\mathcal{A}(E)=\begin{cases}\frac{1}{\pi}\dfrac{\Gamma(E)}{(E-E_b-\gamma^2 g(E))^2+\Gamma(E)^2} & \text{if } \nu(E)\neq0\\ \delta(E-E_b-\gamma^2 g(E)) & \text{if } \nu(E)=0\end{cases} \tag{8}$$

where $\Gamma(E):=\gamma^2\pi\nu(E)$. Within the continuum (that is, $\nu(E)\neq0$), equation (8) can qualitatively be interpreted as a Lorentzian with an energy-dependent half-width at half-maximum (HWHM) $\Gamma(E)$, and an energy-dependent mean $E_b+\gamma^2 g(E)$. Note that for $g(E)$ to be well-defined in the continuum, one has to interpret it as a Cauchy principal value.

More precisely, for the left column of Fig. 1, we consider the DOS

$$\nu(E)=\begin{cases}0 & \text{if } E<0\\ \nu_0/\sqrt{E} & \text{if } E>0\end{cases} \tag{9}$$

which is what one expects for the two-particle continuum of a 1D gapped model (see Supplementary Information). A straightforward calculation gives

$$g(E)=\nu_0\int_0^\infty\frac{d\varepsilon}{\sqrt{\varepsilon}\,(E-\varepsilon)}=\begin{cases}-\dfrac{\pi\nu_0}{\sqrt{-E}} & \text{if } E<0\\ 0 & \text{if } E>0\end{cases} \tag{10}$$

We set $\nu_0=1$. In the top left panel of Fig. 1, we take $\gamma=0.2$, whereas in the bottom left panel, $\gamma=0.7$. We consider the hypothetical scenario where the onset of the continuum is at $\omega_{min}=2-\cos(k)$, where k can physically be thought of as (total) momentum. Moreover, we take the bare level to be flat, $\omega_b=2$. In terms of our earlier variable, where the DOS has its onset at $E=0$, we can thus say that $E_b=\omega_b-\omega_{min}=\cos(k)$.

For the right column of Fig. 1, we consider the DOS

$$\nu(E)=\begin{cases}0 & \text{if } E<0 \text{ or } E_m<E\\ \nu_0\sqrt{E(E_m-E)} & \text{if } 0\leq E\leq E_m\end{cases} \tag{11}$$

which is what one expects for the two-particle continuum of a 3D gapped model (see Supplementary Information). This has a square-root onset at $E=0$ and a square-root termination at $E=E_m$. We obtain

$$g(E)=\begin{cases}\pi\nu_0\,(E-E_m/2) & \text{if } 0<E<E_m\\ \pi\nu_0\,(E-E_m/2-E\sqrt{1-E_m/E}\,) & \text{otherwise}\end{cases} \tag{12}$$

Given our earlier results, we know that there will not always be an isolated state below the continuum. Instead, there is a threshold value $\gamma_{th}=\sqrt{E_b/|g(0^-)|}=\sqrt{2E_b/(\pi\nu_0E_m)}$. If $E_b>0$, an isolated state exists below the continuum if and only if $|\gamma|>\gamma_{th}$.

We again consider $\nu_0=1$, $\omega_{min}=2-\cos(k)$ and $\omega_b=2$, but now we also have to choose an upper threshold energy: $\omega_{max}=5+\cos(k)$. The top right panel of Fig. 1 has $\gamma=0.2$, whereas the bottom right panel has $\gamma=0.5$. We note that the minimum interacting strength for which there is a state below the continuum for all values of k is

$$\gamma=\sqrt{\frac{2}{\pi\nu_0}}\times\sqrt{1/(2+3\sec(k))}\;|_{k=0}=\sqrt{2/5\pi}\approx0.357$$

Finally, with regard to Fig. 1, we mention that we also plot the real part of complex poles when they exist. We see that their location nicely agrees with where the intensity of $\mathcal{A}(E)$ is largest. Moreover, the data in Fig. 1 have been convoluted with a Gaussian with $\sigma=0.025$ (in units shown). This is to give the delta function outside the continuum a visible width.

Ising ladder. In Fig. 2b, we plot the dynamical spin structure factor $\mathcal{S}^{xx}(k,\omega)=\frac{1}{2\pi}\int\langle0|\hat{\sigma}^x_{A,-k}(t)\hat{\sigma}^x_{A,k}(0)|0\rangle e^{i\omega t}dt$ of the spin-$\frac{1}{2}$ ladder defined in the main text. This quantity is very useful, as similarly to $\mathcal{A}(E)$ considered in the solvable model, it tells us about weight on energy eigenstates. More precisely, $\mathcal{S}^{xx}(k,\omega)=\sum_n\delta(\omega-\omega_n)|\langle n|\hat{\sigma}^x_{A,k}|0\rangle|^2$. We calculated these dynamical spin–spin correlations by first using DMRG to obtain the ground state[18] and subsequently time-evolving $\sigma^x_{A,k}|0\rangle$ using a matrix-product-operator-based method[19,20]. We found that a timestep truncation of $dt=0.1$ and a low bond dimension of $\chi=30$ was enough to achieve converged results. We used linear prediction[34] and multiplication by a Gaussian to soften the effects of Fourier-transforming a finite-time window. This introduces an effective broadening corresponding to a convolution with a Gaussian with $\sigma=0.055$ in the units shown in Fig. 2.

The values of the parameters for the top panel in Fig. 2b are $g_B=0.5$, $J_B=1$ and $\gamma=0.3$. If we now ramp up the coupling strength γ, however, this effectively renormalizes the parameters of the Ising chain. This is because $\hat{H}_{int}$ is not purely an interaction term: it contains an $\hat{S}_z$ on the Ising chain, which attempts to condense the domain walls and cause a phase transition. To prevent this, while ramping up γ we also change parameters J_B and g_B such that the location of the continuum (shaded region in Fig. 2b) remains roughly unchanged. Thus, for the bottom panel, we arrive at $g_B=0.9$, $J=3$ and $\gamma=3.4$. The location of the continuum was determined by numerically extracting the dispersion of a single domain wall.

Dynamics of the TLHAF. In Fig. 3a, we consider the out-of-plane dynamical spin structure factor $\mathcal{S}^{yy}(\mathbf{k},\omega)=\frac{1}{2\pi}\int\langle0|\hat{\sigma}^y_{-\mathbf{k}}(t)\hat{\sigma}^y_{\mathbf{k}}(0)|0\rangle e^{i\omega t}dt$ of the Hamiltonian in equation (2), where we take the 120° order to be in the x–z plane. This can be obtained by the methods mentioned in the case of the Ising ladder (including linear prediction), extended to the case of cylindrical geometry (for more details, see refs. [27,28]). For the data in this work, the cylinder has circumference $L_{circ}=6$, taking the periodic direction to be along one of the primitive vectors. We checked that while the multimagnon continuum still has a dependence on L_{circ}, the single-magnon dispersion is better converged in L_{circ}—at least for the middle- and high-energy modes of interest. One way we checked this is by comparing the energies at points that are equivalent in 2D but not on the cylinder geometry, and finding that they agree.

Due to the absence of continuous symmetry in the ground state, the large coordination number of the lattice and the fact that the isotropic point has three Goldstone modes, it is numerically challenging to time-evolve this highly entangled state. For this reason we are limited in the bond dimensions that we can reach: $\chi=450$ for the long-time dynamics necessary for resolving high-energy modes, and $\chi=800$ for short-time dynamics for low-energy modes (see discussion in the following).

The numerical parameters for Fig. 3a correspond to a timestep truncation $dt=0.05J$, bond dimension $\chi=450$ and an effective Gaussian broadening with $\sigma=0.077J$. The dotted line in Fig. 3a is the sum $\varepsilon_{\mathbf{q}}+\varepsilon_{\mathrm{K}}$, where $\mathbf{q}$ is along the orange line in the inset. Here $\varepsilon_{\mathbf{q}}$ was obtained by tracing the peak of the spectral function along that slice, and ε_{K} is a low-energy feature that could not be resolved with bond dimension $\chi=450$. Instead, we went up to $\chi=800$, which limited the time window we could obtain, leading to larger effective broadening. However, because the low-energy mode is well-separated from other (relevant) modes, one can still reliably extract the energy from a broad response. From a scaling in bond dimension, we then obtained $\varepsilon_{\mathrm{K}}\approx 0.3J$ for the value $\delta=0.05$. This extrapolation is represented visually in the Supplementary Information. This is markedly lower than the LSWT prediction, $\varepsilon_{\mathrm{K}}^{\mathrm{LSWT}}\approx 0.41J$.

The magnon dispersion in Fig. 3c was obtained by tracing the low-energy peak of the spectral function, having verified that the magnon branch was resolved enough for this to be sensible. At low energies, this was supplemented by the aforementioned approach where we could go up to $\chi=800$. Due to the cylindrical geometry on which our method is based, the dispersion we obtain is continuous along one direction and discrete along the other. We then superimposed the momentum cuts along three different orientations and subsequently interpolated this to the full 2D Brillouin zone (see Supplementary Information). The fact that where these cuts intersected they agreed is a confirmation that the circumference $L_{\mathrm{circ}}=6$ is large enough for the single-magnon dispersion to resemble the true 2D result. As a sanity check for our interpolation method, we verified that it gives the correct result when applied to the LSWT dispersion, as shown in the Supplementary Information .

We present a detailed analysis of the convergence of our results in both bond dimension and cylinder circumference in the Supplementary Information.

Experimental data for the TLHAF. In the inelastic neutron scattering data for $Ba_3CoSb_2O_9$ in Fig. 4a, the momentum cut is along K–K′. In the inset of Fig. 3a, K′ is shown as a corner point of the (first) Brillouin zone. However, in the experiment[2], K′ was taken in the second Brillouin zone (which differs from the other choice by a reciprocal lattice vector). This difference has no bearing on the bands one picks up, so for our purposes this distinction is irrelevant. It does, however, affect the precise value of the intensity. This explains why Fig. 4a is not left–right symmetric.

Subtleties near and at the isotropic point of the TLHAF. The decay process $\mathbf{k}\to \mathrm{K}+(\mathbf{k}-\mathrm{K})$ accounts for the complete decay region (as predicted by LSWT) only at the isotropic point ($\delta=0$). For $\delta\neq 0$, this process represents the core of the decay region, which is then slightly extended by considering $\mathbf{k}\to\mathbf{q}+(\mathbf{k}-\mathbf{q})$ with $\mathbf{q}\approx$ K. One consequence is that the minimum predicted by the principle of avoided decay is only precisely at Y_1 at the isotropic point. Indeed, in Fig. 3c one can see that the minimum (for $\delta=0.05$) has been slightly shifted inward, albeit not very substantially so.

Interestingly, at the isotropic point $\delta=0$, absence of decay is equivalent to the magnon dispersion $\varepsilon_{\mathbf{k}}$ being periodic with respect to the magnetic Brillouin zone—which is three times smaller than the original Brillouin zone. (This can be derived from the fact that $\varepsilon_{\mathrm{K}}=0$ for $\delta=0$). This powerful criterion might help to figure out the extent of (avoided) decay at the isotropic point, be it using numerical or experimental methods.

Relationship between E_{b}, $E^{\star}$ and Z. In the main text, we alluded to the general relationship $\mathrm{d}E^{\star}/\mathrm{d}E_{\mathrm{b}}=Z$. This is a general property of our model. To prove this, first rewrite

$$\frac{\mathrm{d}E^{\star}}{\mathrm{d}E_{\mathrm{b}}}=\frac{\mathrm{d}}{\mathrm{d}E_{\mathrm{b}}}\left\langle \psi^{\star}|\hat{H}|\psi^{\star}\right\rangle=\left\langle \psi^{\star}|\frac{\mathrm{d}\hat{H}}{\mathrm{d}E_{\mathrm{b}}}|\psi^{\star}\right\rangle \tag{13}$$

where we used the Hellmann–Feynman theorem to move the derivative inside. The proof is finished by noting that equation (3) implies $\frac{\mathrm{d}\hat{H}}{\mathrm{d}E_{\mathrm{b}}}=|\psi\rangle\langle\psi|$.

Predictions for helium. Finally, we make a few comments relevant to the case of superfluid helium. As shown in the Supplementary Information, the two-roton continuum has a jump discontinuity . Hence, let us consider the case where $\nu(E)$ has a discontinuous onset ν_0. A straightforward computation then shows that $g(E)\approx\nu_0\ln(-E)+\mathrm{const}$, for E small and negative. Hence, remembering the condition we derived above ($E^{\star}=E_{\mathrm{b}}+\gamma^2 g(E^{\star})$), we see that as $E^{\star}\to 0^{-}$, we have the functional relationship $\nu_0\ln(-E^{\star})=E_{\mathrm{b}}+\mathrm{const}$, that is, $E^{\star}\propto\exp(-E_{\mathrm{b}}/\nu_0)$. Using the fact (see Supplementary Information) that $\nu_0\approx 1/k$, we obtain the formula mentioned in the main text. Using the general relationship $\mathrm{d}E^{\star}/\mathrm{d}E_{\mathrm{b}}=Z$, we also directly obtain the other prediction. In particular, this means that the values of a and b (the parameters mentioned in the caption of Fig. 4) should be equal. However, it does not make sense to expect this for the experimental data, as the weight Z extracted in that setting is usually only defined up to a global multiplicative factor.

Experimental data for helium. With regard to the experimental data for helium, the quasiparticle dispersion relation was straightforwardly extracted from refs. [4,5]. The weight, however, is more subtle (refs. [6,7] show the data as a function of momentum, which we extracted and interpolated). We then evaluated this interpolated function at the same momenta for which refs. [4,5] quoted values for the energy. This allowed us to plot Z as a function of energy in the inset of Fig. 4d.

Data availability

The data that support the findings of this study are available from the corresponding author upon request.

Code availability

Details about the DMRG code are provided in the Methods and in the Supplementary Information.

References

33. Zimering, S. Some asymptotic behavior of Stieltjes transforms. *J. Math. Phys.* **10**, 181–183 (1969).
34. White, S. R. & Affleck, I. Spectral function for the $S=1$ Heisenberg antiferromagetic chain. *Phys. Rev. B* **77**, 134437 (2008).